Electronic Supplementary Material (ESI) for Journal of Materials Chemistry C.

— Electronic Supplementary Information —

Extrinsic doping of Hg_2GeTe_4 in the face of defect compensation and phase competition

Claire E. Porter,*,† Jiaxing Qu,*,‡ Kamil Ciesielski,† Elif Ertekin,‡ and Eric S. Toberer†

†*Colorado School of Mines, Golden, CO 80401*

‡*University of Illinois at Urbana-Champaign, Urbana, IL 61801*

E-mail: c7porter@gmail.com; jiaxing6@illinois.edu

* equal contributions

1. DOS Edge for Dopants

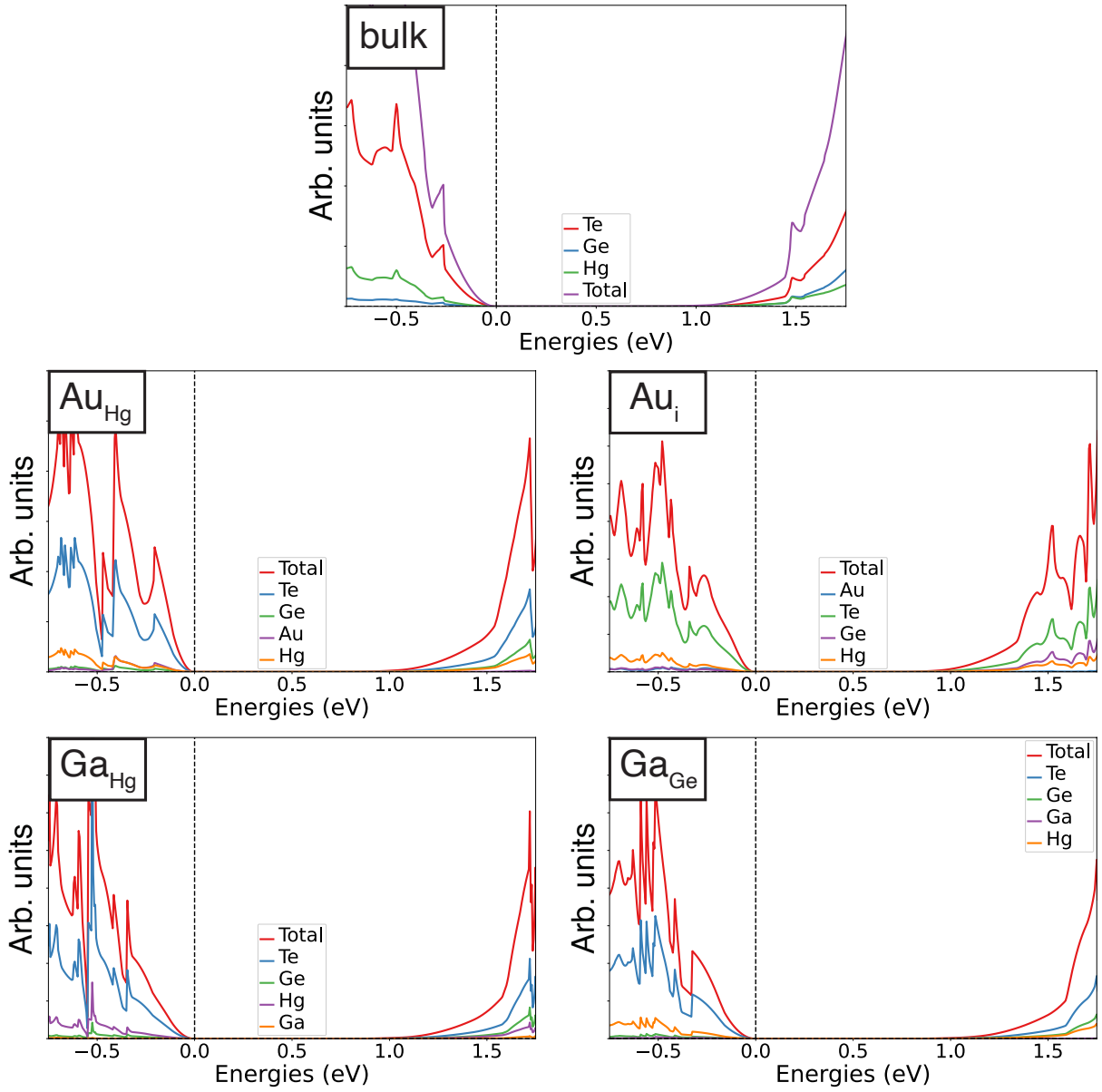

Figure S1: Comparison of density-of-states for undoped and doped Hg_2GeTe_4 around band edges. Example shown for Au- and Ga-doped Hg_2GeTe_4 supercell with the lowest acceptor and donor defects. Minimal change in band edge shape indicates the validity of rigid band approximation.

2. Defect diagram for Ag and Au under Hg-rich growth condition

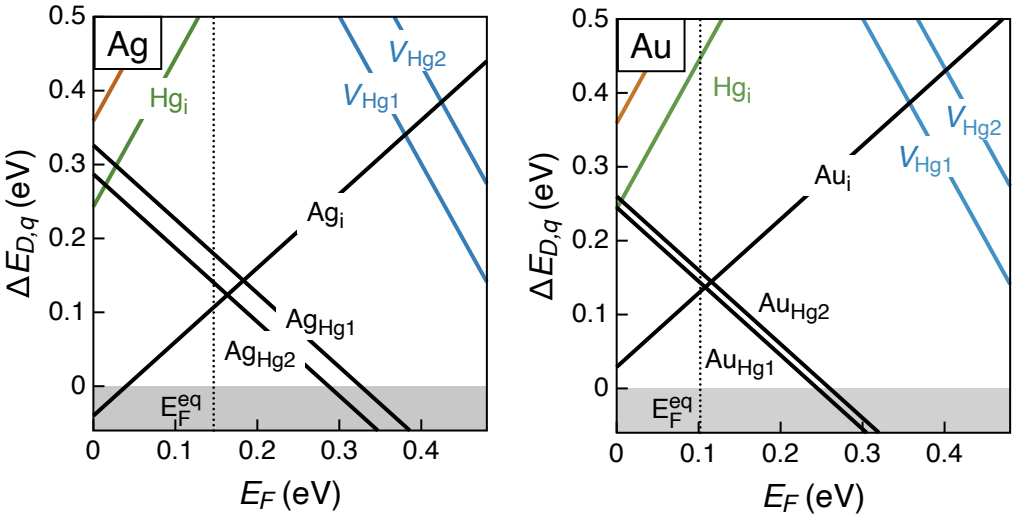

Figure S2: Defect diagram for Ag and Au-doped Hg_2GeTe_4 under Hg-rich growth condition.

3. Dopant chemical potential and lowest energy defect

Table S1: Dopant chemical potential ($\Delta\mu_D$, eV/atom) under two thermodynamic states (1 = Hg-rich/Ge-rich and 2 = Hg-poor/Ge-rich). The lowest energy defect ($\Delta H_{D,q}$, eV/defect) at a Fermi level $E_F = 0.24$ eV is shown for all dopants. High chemical potential is not the sole factor in driving high energy defects (i.e. Sb, Bi form defects about 10 times higher in energy than Cu defets, although Cu is more limited by its chemical potential). *$Cu_2HgGeTe_4$ is known to form a full solid solution with Hg_2GeTe_4.

Dopant	$\Delta\mu_D$, 1	$\Delta\mu_D$, 2	$\Delta H_{D,q}$	Lowest energy defect	Competing phase
Sb	-0.10	-0.27	1.5	Sb_{Ge}^{+1}	Sb_2Te_3
Au	-0.13	-0.35	0.4	Au_{Hg1}^{-1}	$AuTe_2$
Ag	-0.19	-0.26	0.05	Ag_{Hg2}^{-1}	AgTe
Bi	-0.43	-0.60	0.9	Bi_i^{+3}	Bi_2Te_3
Cu	-0.48	-0.56	0.1	Cu_i^{+1}	$Cu_2HgGeTe_4$*
Ga	-0.97	-1.11	0.1	Ga_{Hg1}^{+1}	$HgGa_2Te_4$
In	-1.01	-1.15	0.2	In_{Hg1}^{+1}	$HgIn_2Te_4$
Zn	-1.12	-1.21	0.1	Zn_i^{+2}	ZnTe
Li	-1.99	-2.05	0.2	Li_{Hg2}^{-1}	Li_2Te
Sc	-2.54	-2.65	0.1	Sc_{Hg1}^{+1}	ScTe
Mg	-2.83	-2.94	1.1	Mg_i^{+2}	MgTe
Br	-3.20	-3.10	2.6	Br_{Te}^{+1}	Hg_3Br_4Te
Na	-3.47	-3.81	1.9	Na_{Hg2}^{-1}	$NaTe_3$
I	-3.94	-3.80	3.9	I_{Te}^{+1}	$Hg_3I_2Te_2$
La	-4.11	-4.26	1.1	La_{Hg2}^{+1}	La_3Te_4
Y	-4.93	-5.10	1.3	Y_{Hg2}^{+1}	Y_2Te_3

3. Doping efficiency for Au, Ag, Li, Cu, Sc, Zn, In, Ga

Table S2: Doping efficiency (η)

	Growth conditions	
Dopant	Hg-poor/Ge-rich	Hg-rich/Ge-rich
Cu	49%	49%
Li	50%	48%
Ag	49%	49%
Au	61%	85%
In	99%	87%
Zn	0.030%	0.036%
Sc	95%	71%
Ga	52%	51%

Doping efficiency for the eight candidate dopants of the main study. Calculations are discussed in Section 1.2.1 Doping Efficiency. The top four rows (Cu, Li, Ag, and Au) show efficiency for p-type doping, and the bottom rows (In, Zn, Sc, and Ga) are for n-type doping. The doping efficiency is only one predictor in electronic transport; for example, while Ag and Au have much lower doping efficiencies than n-type dopants In and Sc, the former dopants are more successful at increasing the carrier concentration due to the low energy defects they form and the native p-type nature of Hg_2GeTe_4.

5. Au-doped SEM & XRD

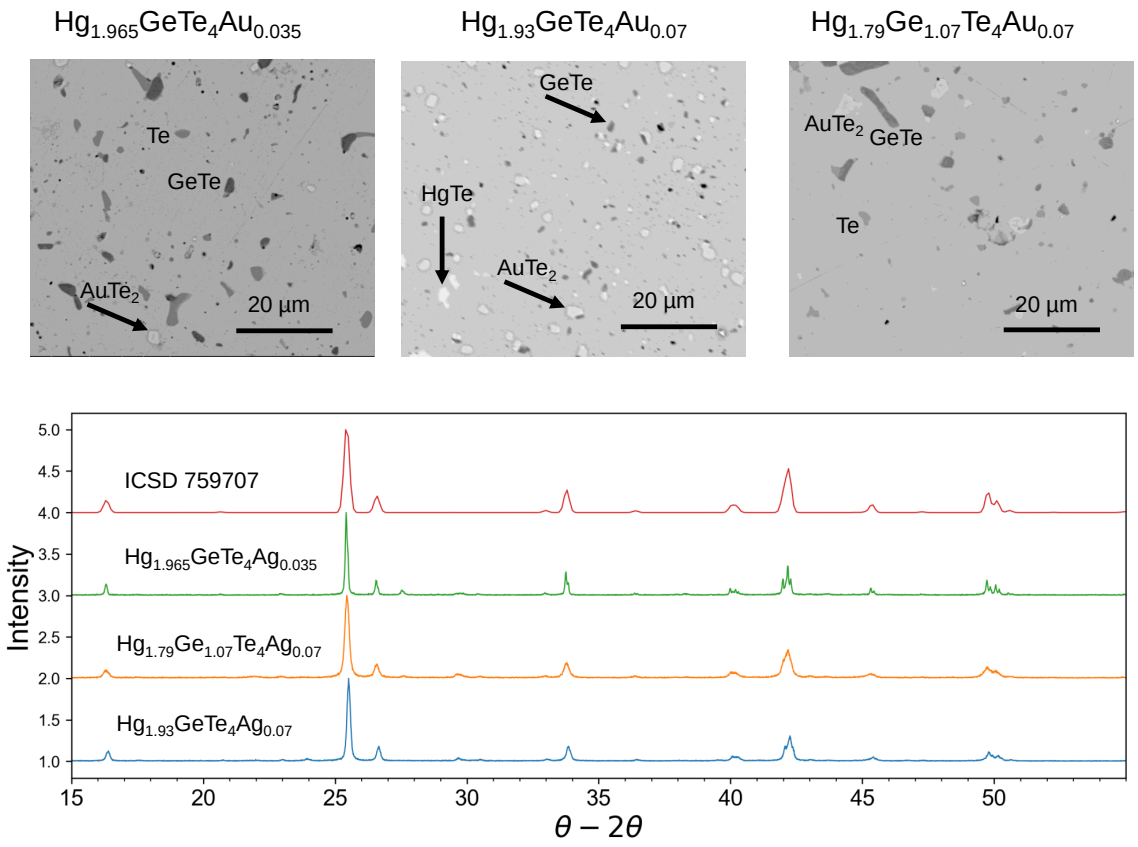

Figure S3: Trace amounts of impurity phases (GeTe, HgTe, Te, $AuTe_2$) are found via SEM/EDS and pin the sample in chemical potential space to a chemical invariant point. The main matrix phase (light grey) is Hg_2GeTe_4. Overall sample homogeneity is excellent, evidenced by XRD.

6. Ag-doped SEM & XRD

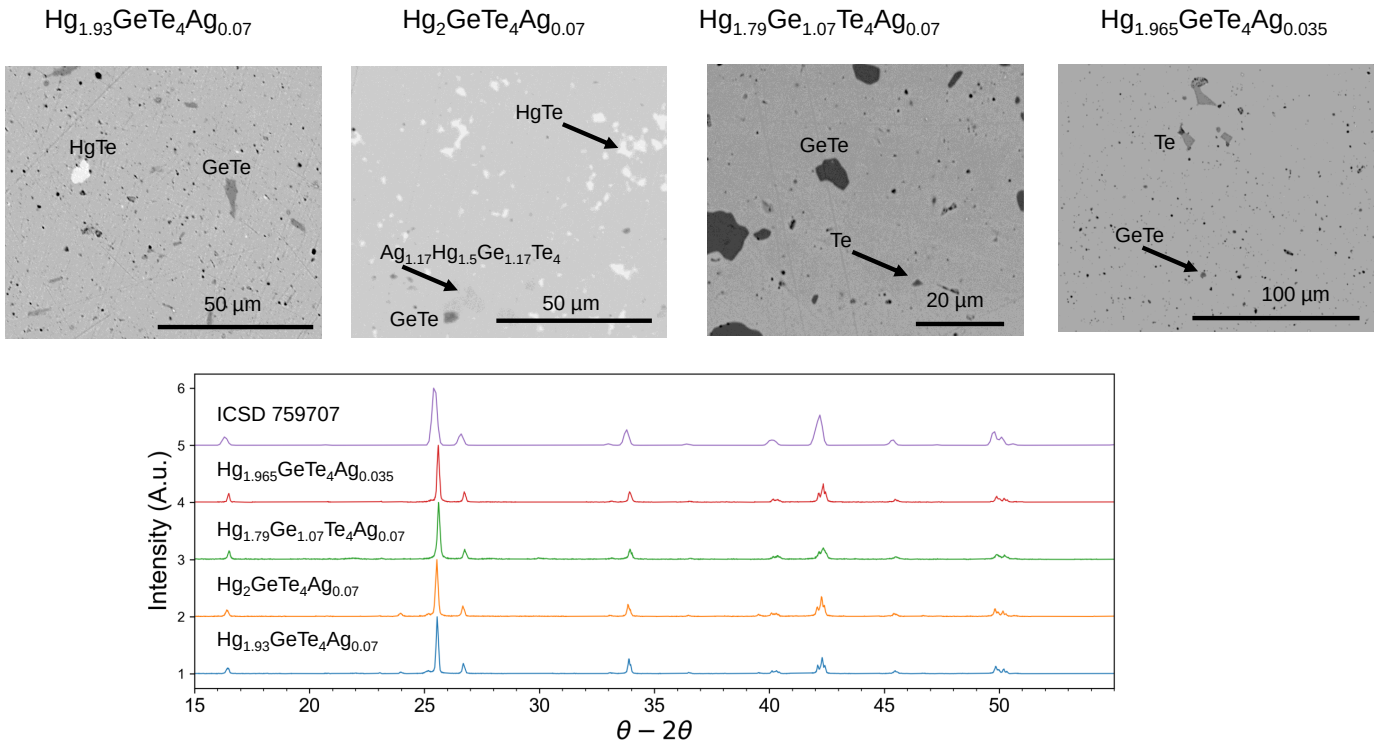

Figure S4: Ag doping generates good quality samples and subtle shifts in the stoichiometry produce different native impurity phases as well an unreported quaternary phase $Hg_2GeTe_4Ag_{0.07}$. The main matrix phase (light grey) is Hg_2GeTe_4.

7. Cu-doped SEM & XRD

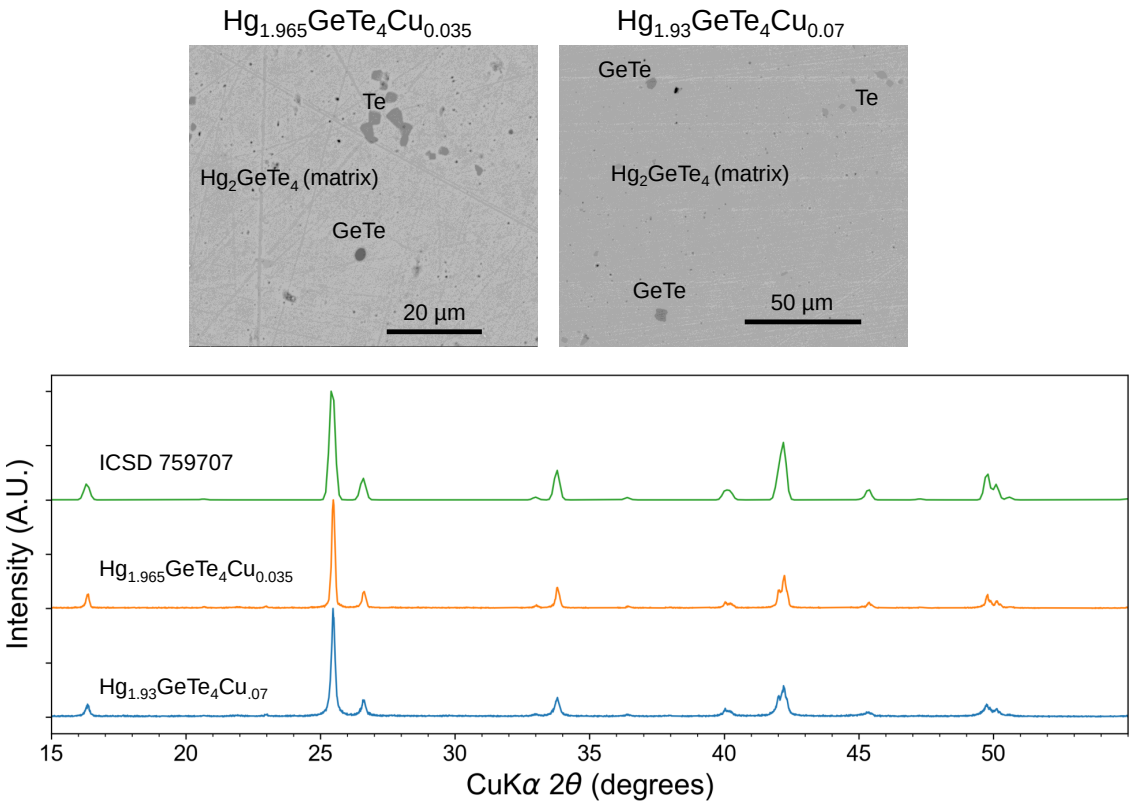

Figure S5: The SEM and XRD for Cu-doped samples show very homogeneous samples with excellent density (negligible porosity in SEM) and minimal trace impurity phases. The main matrix phase (light grey) is Hg_2GeTe_4.

8. Zn, In, Sc-doped samples SEM & XRD (main text samples; transport in Figure 6)

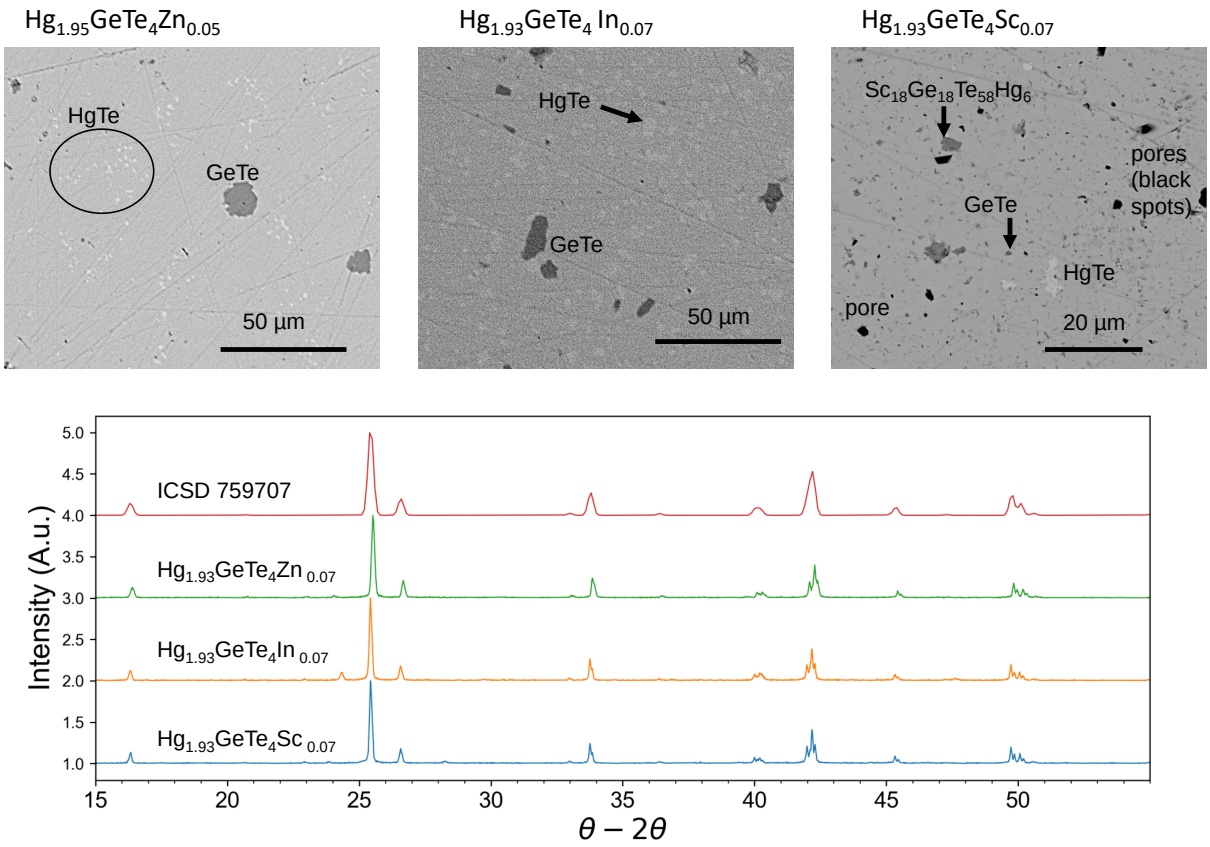

Figure S6: Samples doped with Sc, In, and Zn that are featured in the main text (Figure 6). The main matrix phase (light grey) is Hg_2GeTe_4.

9. Ga, Zn, Sc-doped samples (not main text) SEM & XRD

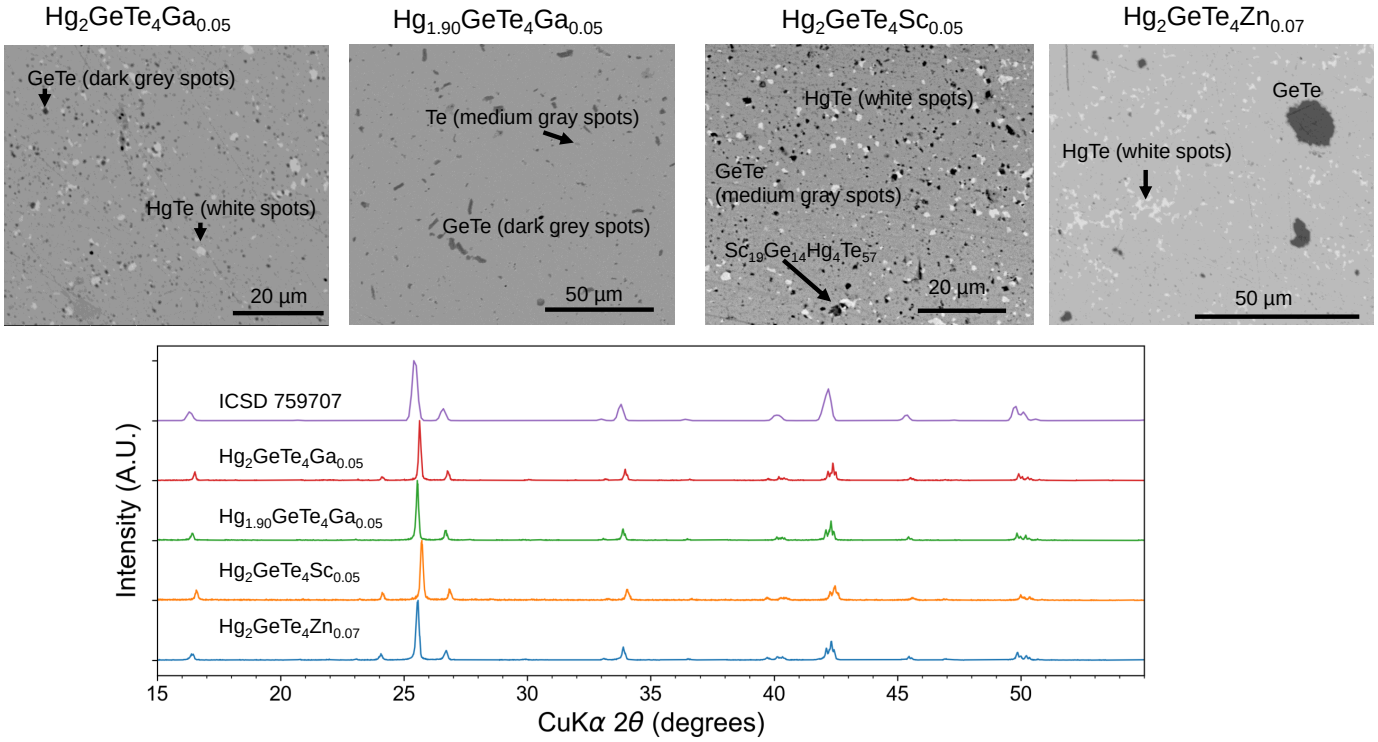

Figure S7: These samples are not included in the main text because it is likely that they contain excess amounts of HgTe that influences transport due to its very strong electron mobility (Figure S11). $Hg_{1.90}GeTe_4Ga_{0.05}$ does not fall under this category and is ommitted from the main text for clarity. Small peaks in the XRD patterns at 24° denote the presence of HgTe, which is reflected in the SEM images as well (white spots are HgTe). Transport data for these samples are shown in Figure S10 and S9. The main matrix phase (light grey) is Hg_2GeTe_4.

10. Cu-doping electronic transport

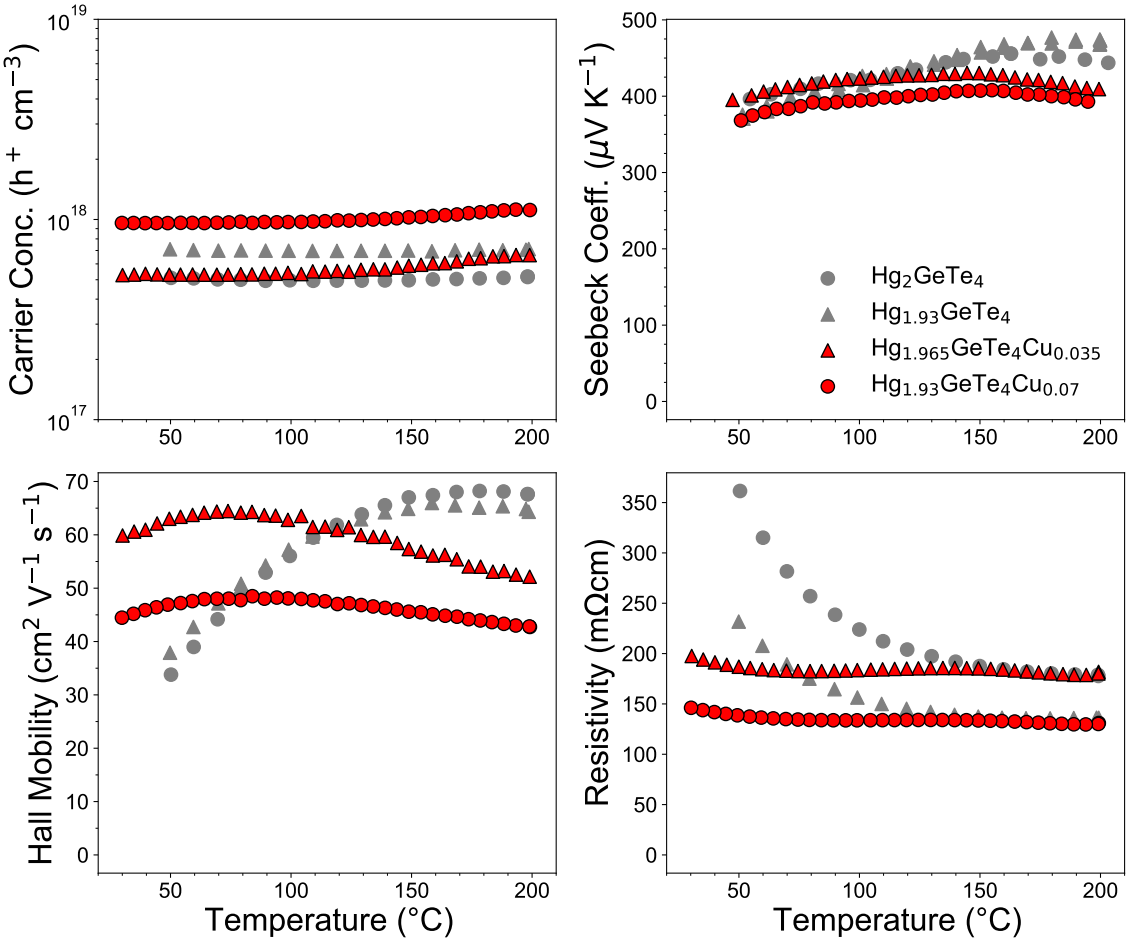

Figure S8: Cu is largely ineffective as an extrinsic dopant in Hg_2GeTe_4.

11. Ga-doping electronic transport

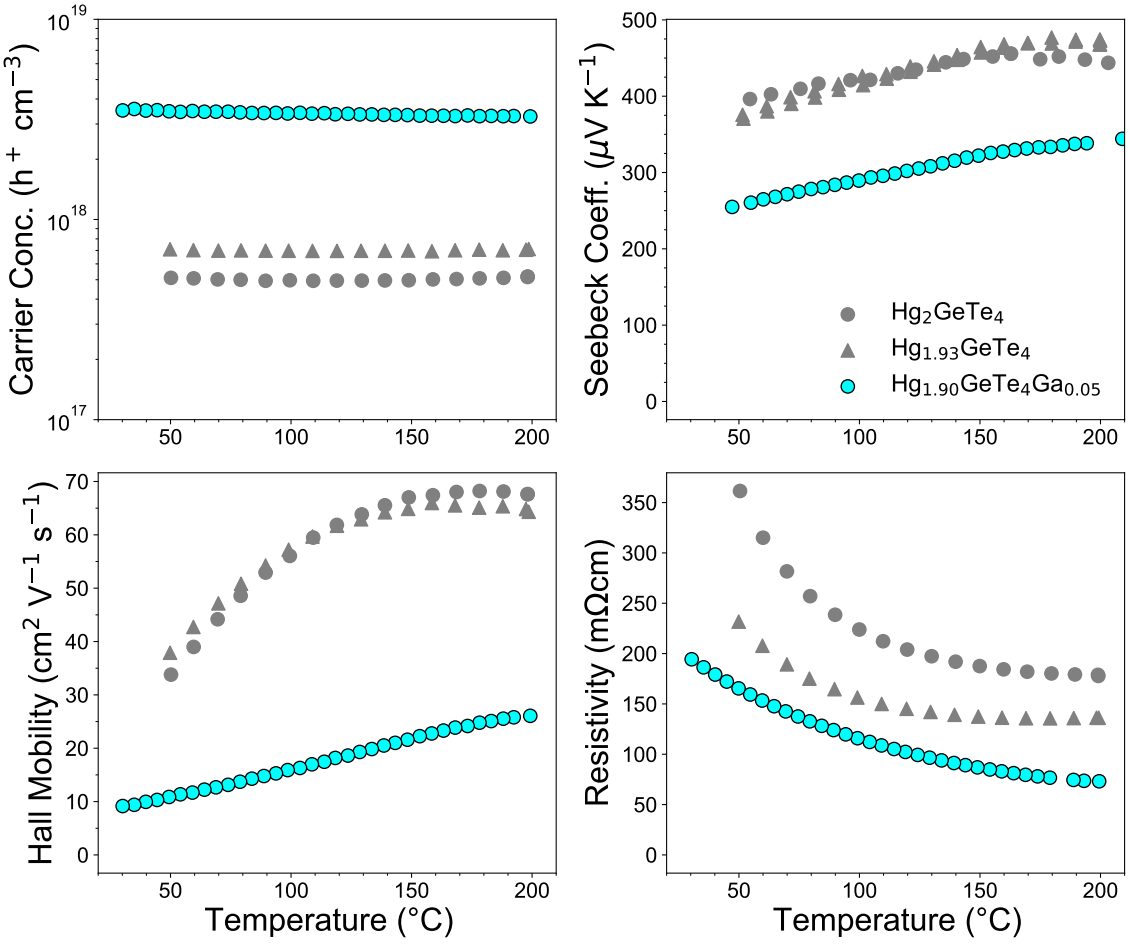

Figure S9: Under Hg-poor conditions as seen here, Ga-doping generates *p*-type electronic transport. The Hall mobility is quite low and is likely limited by ionized impurity scattering.

12. Bipolar samples: Sc, Ga, Zn

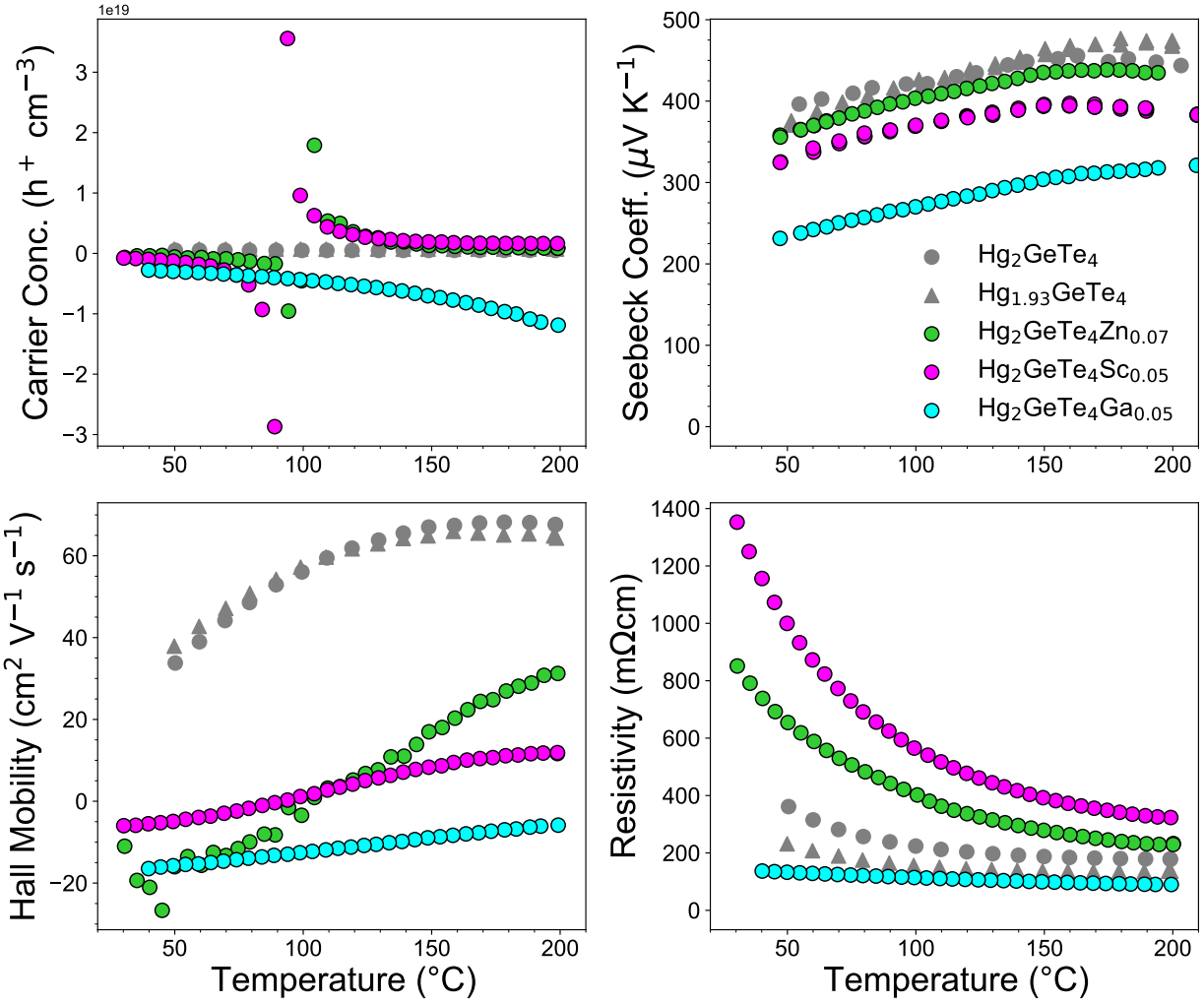

Figure S10: Bipolar data for samples doped with Sc, Ga, and Zn. Not all samples doped with these elements were bipolar, as discussed in main manuscript.

14. HgTe Hall Transport

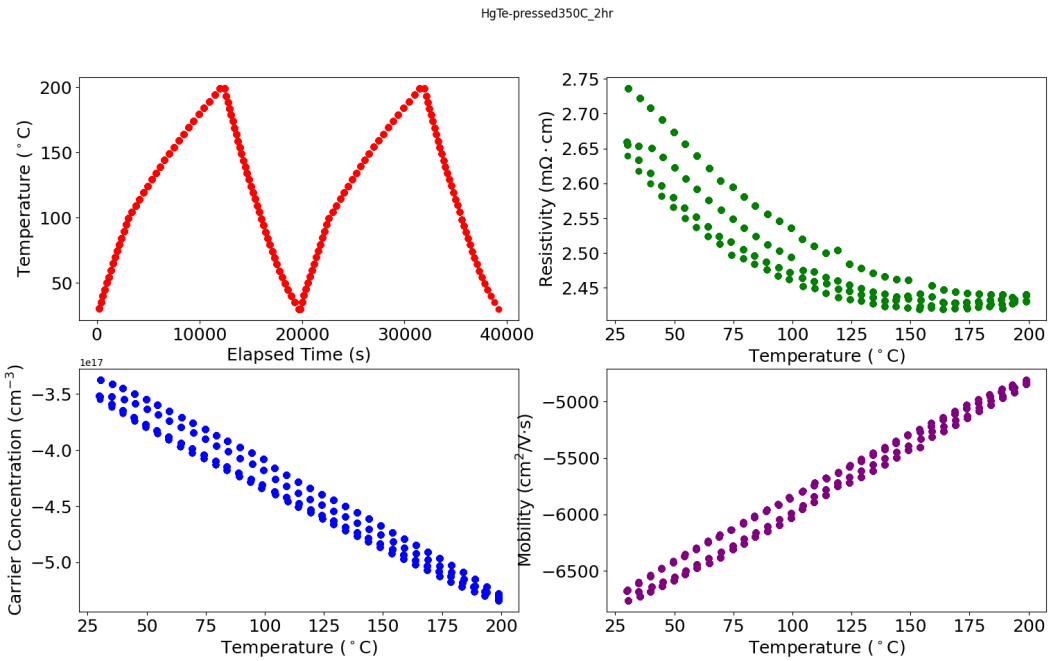

Figure S11: HgTe has very high intrinsic mobility and low resistivity. The presence of this binary compound is required by phase boundary mapping of Hg_2GeTe_4 under Hg-rich conditions, but too much of it can lead to a false positive of n-type results.

15. Defect Diagrams with band-edge 'defects'

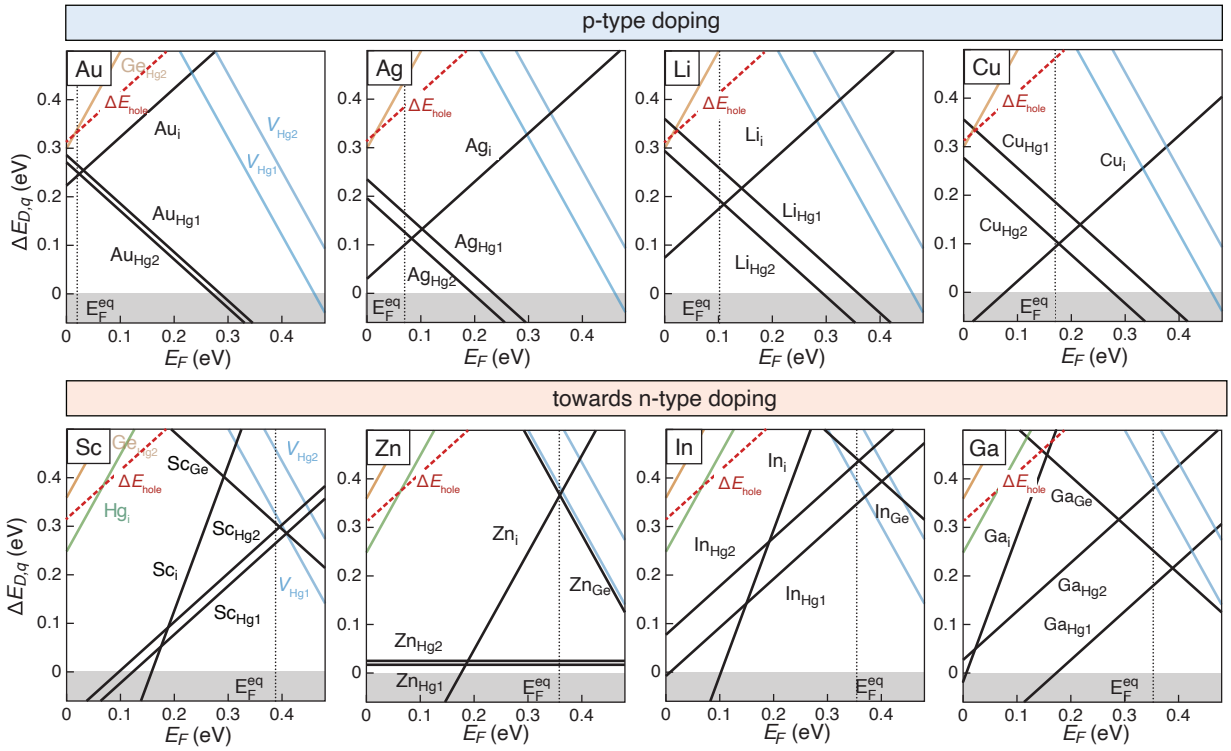

Figure S12: Calculated formation energies of native point defects as well as the band-edge 'defects' as functions of Fermi levels in Hg_2GeTe_4. The virtual 'hole defect' is shown by the dashed red line. The virtual 'electron defect' has high formation energy (1.06 eV at VBM) and does not appear in this diagram. With such visualization, it is demonstrated that doped Hg_2GeTe_4 is a defect-dominant system where the equilibrium Fermi energy is largely determined by low energy defects.